A MULTI-SCALE INVESTIGATION OF THE MECHANICAL BEHAVIOR OF DURABLE SISAL FIBER CEMENT COMPOSITES

Flávio de Andrade Silva[1], Romildo D. Toledo Filho[2], Barzin Mobasher[3] and Nikhilesh Chawla[4]

Summary:

Durable sisal fiber cement composites reinforced with long unidirectional aligned fibers were developed and their mechanical behavior was characterized in a multi-scale level. Tensile tests were performed in individual sisal fibers. Weibull statistics were used to quantify the degree of variability in fiber strength at different gage lengths. The fiber-matrix pull-out behavior was evaluated at several curing ages and embedded lengths. The composite's mechanical response was measured under direct tension while crack formation was investigated using a high resolution image capturing procedure. Crack spacing was measured using image analysis and correlated with the applied strain under both the tensile and bending response.

Keywords: sisal fibers, cement composites, mechanical properties.

1. Introduction

The development of durable, strong, and ductile composites for construction applications could solve the problem of shelter for millions of people living in sub-standard conditions. Addressing key technical hurdles and presenting solution strategies to improve the manufacturing, characterization, analysis, and design of innovative structural composites made from natural fibers will enable a broad scale global application. The opportunity to develop low cost construction materials with locally and indigenously produced sustainable agricultural fibers will have long term social and economical consequences.

This paper addresses the development of strain hardening cement composites using sisal, a natural fiber with an average tensile strength of 400 MPa and strain at failure of 3% as reinforcement in concrete. These composites provide an exciting opportunity to the housing construction industry and may generate economic incentives particularly in developing countries since the availability and production of composite reinforcement requires a low degree of industrialization. Furthermore, in comparison to the most common synthetic reinforcing fibers, natural fibers require less energy to produce and are the ultimate green products.

Natural fibers have been traditionally used as a substitute of asbestos in the form of chopped, short, and or in a pulp form for the production of thin elements for roofing and cladding. An increased use of these materials for applications such as cladding, internal, and external partitioning walls is possible and may lead towards the development of low cost sustainable materials [1-8]. Nevertheless, their application in the construction industry is still quite limited due to the lack of understanding in how to improve the durability while making ductile materials.

Continuous fiber reinforced cement based composites are a new class of sustainable construction materials with superior tensile strength and ductility [9-10]. The enhanced strength and ductility is primarily governed by the composite action that exists such that the fibers bridge the matrix cracks and transfer the loads, allowing a distributed microcrack system to develop. These materials are strong enough to be used as load bearing structural members, in applications such as structural panels, impact & blast resistance, repair and retrofit, earthquake remediation, strengthening of unreinforced masonry walls, and beam-column connections [11].

A fundamental understanding of the structural behavior in the three different levels of continuous natural sisal fiber composite system (i.e. micro, meso and macro) is important for analysis, modeling and design. The present paper addresses the mechanical behavior of the reinforcement, its interface with the cement matrix and the macro behavior of the composite.

2. Experimental Program

2.1 Materials and Processing

To produce durable natural fiber composites, the cementitious matrix consisted of 50% Portland cement, 30% metakaolin (MK) and 20% calcined waste crushed clay brick (CWCCB) following previous works [12]. The matrix was produced using the Portland cement CPII F-32 defined by the Brazilian standard [13] as composed with filler (in mass: 85%<clinker<91%; 3%<gypsum<5%; 6%<filler<10%) with a 28 days compressive strength of 32 MPa. The metakaolin (MK) was obtained from Metacaulim do Brasil Industria e Comércio LTDA, and calcined waste crushed clay

brick (CWCCB) from an industry located in Itaborai – RJ, Brazil, calcined at 850 $^{\circ}$C. River sand with maximum diameter of 1.18 mm and density of 2.67g/cm^3 and a naphthalene superplasticizer Fosroc Reax Conplast SP 430 with content of solids of 44% were used.

The mortar matrix used had a mix design of 1:1:0.4 (cementitious material:sand:water by weight). Wollastonite fiber (JG class), obtained from Energyarc, were used as a micro-reinforcement in the composite production (V_f = 5%).

The matrix was produced using a bench-mounted mechanical mixer of 20 liters capacity. The cementitious materials were homogenized by dry mixing for 30 seconds prior to addition of sand and 5% by volume of wollastonite. The dry ingredients were mixed for an additional 30 seconds prior to addition of superplasticizer and water. The mixture was blended for 3 minutes. For the production of the laminates, the mortar mix was placed in a steel mold, one layer at a time, followed by single layers of long unidirectional aligned fibers (up to 5 layers). The samples were consolidated using a vibrating table operated at a frequency of 65 Hz, resulting in a sisal fiber volume fraction of 10%. After casting the composites were compressed at 3 MPa for 5 minutes.

Special molds were designed for casting single filament pullout specimens. PVC tubes were used as the formwork while wooden bases were used to guarantee the accuracy of the sisal fiber orientation at the centroidal axis of the mold through a hole drilled at the center of the base plate. The sisal fiber was inserted through the eye of a needle, which was then contrived through the wooden mold. The mix was then poured into the PVC tubes in three layers followed by manual compaction. The specimens were covered in their molds for 24 hours prior to moist curing for 28 days in a cure chamber with 100% RH and 23±1 ^{0}C.

2.2 Mechanical characterization of sisal fibers

The as-received fibers were tested, in a natural dry condition, under tensile loading at four different gage lengths (GL): 10, 20, 30, and 40 mm. Testing was conducted on a microforce testing system (Tytron 250, MTS Systems, Minneapolis, MN). A steel "V" shaped mechanical clamping grip was used to grip the fibers. A 250 N load cell was used to measured load. The displacement of the fiber was measured using a short-stroke transducer with a resolution of about 0.1 µm. Tensile tests were conducted in displacement control at a rate of 0.1 mm/min. All testing was conducted at ambient temperature (~22 ^{0}C) and a relative humidity of about 20%.

The compliance of the loading and gripping system was determined by obtaining the force versus displacement behavior of the fiber at various gage lengths following the methodology used elsewhere. [14].

2.3 Interfacial Characterization

An electromechanical MTS (model SINTECH 1/S) was used for the pullout tests. The PVC mold was connected to a 0.44 kN load cell that was attached to the crosshead. The bottom part consisted of a pinch grip where the free end of the fiber was tightened. The test was conducted under constant crosshead displacement control at a rate of 0.1 mm/min. Six specimens of embedment length ranging from 10 to 40 mm were tested after 3 days of curing. To investigate the influence of curing age on the

fiber-matrix bond strength specimens with embedment length of 20 mm were tested at ages ranging from 3 to 28 days.

2.4 Mechanical characterization of sisal fiber reinforced composite

Direct tensile tests were performed in a closed loop servohydraulic testing machine with a capacity of 500 kN. The tests were controlled by the cross-head displacement at a rate of 0.1 mm/min. Six specimens measuring 400 mm x 50 mm x 12 mm (length x width x thickness) were tested using a gage length of 300 mm with fixed–fixed boundary conditions. Aluminum thin sheets were glued on both ends of the specimen and the pressure of the hydraulic grips was adjusted to 1.37 MPa in order to minimize stress concentration and damage.

By evaluating cracking patterns at regular time intervals, crack development throughout the loading cycle of tensile and bending test were recorded. A digital Pulnix camera with a 10X macro zoom lens and frame grabber captured images of 480 x 640 in resolution at 60 second intervals. Images were used to measure the crack formation during tension tests. More information on the image analysis technique can be found in the author's previous work [15].

2.5 Discussion and Analysis

A total of 15 fibers were randomly chosen from a given batch and tested at each gage length. The Young's modulus was calculated in the elastic portion of the stress-strain curve and then corrected for compliance by measuring force versus displacement, at various gage lengths [14]. The fibers presented an average elastic modulus of 19 GPa and ultimate tensile strength of 400 MPa. The gage length does not seem to influence the modulus of the fiber. Figure 1 (a) shows the "as-measured" versus corrected stress-strain response of the sisal fiber. At a given stress the contribution of the machine compliance resulted in larger displacements. It should also be noted that the calculation of the modulus from the corrected curve resulted in similar values compared to the modulus computed from the displacement/force versus gage length procedure. A non-linear region, following the initial portion of the stress-strain curve, was observed for some of the tested fibers. This behavior is due to a collapse of the weak primary cell walls and delaminate between fiber cells [14]. The strain-to-failure of the fibers decreased with increasing gage length. This behavior is related to the average size and distribution of flaws in the volume of the fiber.
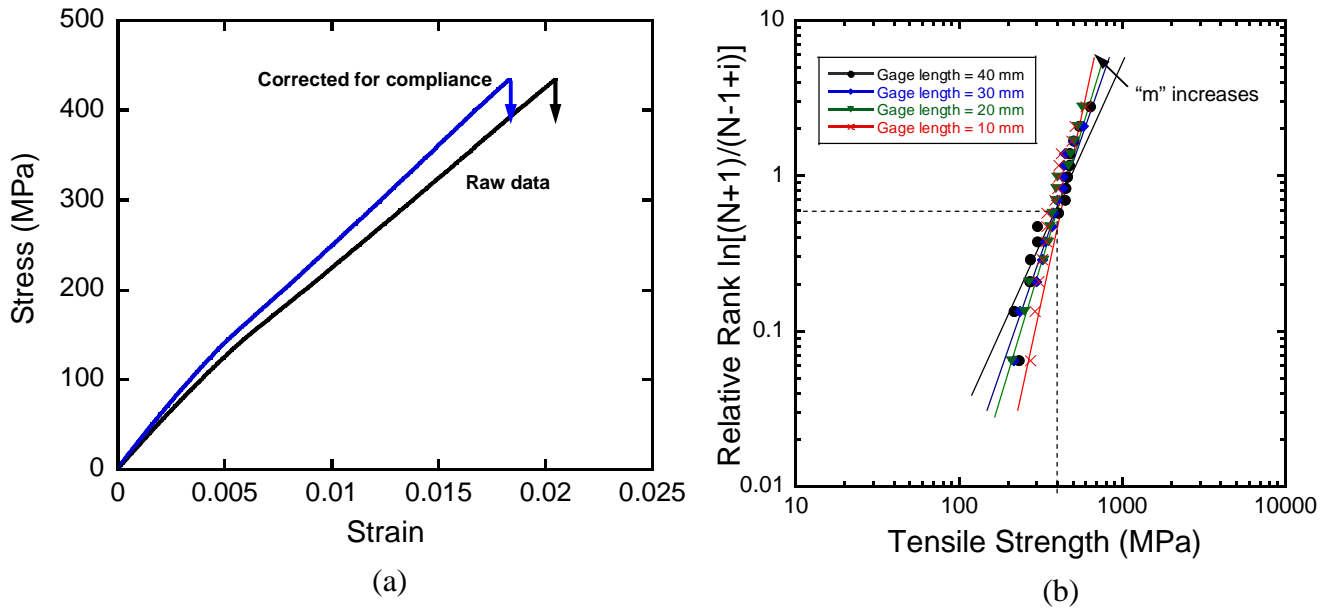
Figure 1. Tensile behavior of natural sisal fibers: (a) Stress vs. strain curve and (b) effect of gage length on the weibull modulus.

Figure 1 (b) shows the influence of gage length on the Weibull modulus "m". Increasing gage length resulted in a decrease in the Weibull modulus. It can be seen from Figure 1 (b) that even though the curves have different slopes (e.g., different values of "m") they all intercept at the same point (e.g., they have the same mean strength). According to Chawla [16], this behavior of different materials having the same mean strength but different Weibull modulus can be explained as follows. The mean defect size for all materials controls the mean strength, but the number of defects controls the Weibull modulus. Thus, while the fibers with a lower gage length have a smaller number of defects, the average defect size is the same as that of the other gage lengths. The question of why strength is not affected by gage length, while the ductility is affected by gage length, may now be explained as follows. The mean flaw size controls the strength, as described above. This mean flaw size does not change with gage length. Once a crack is formed at the largest flaw, how quickly the linkage between flaws occurs will determine the ductility. Thus, if a larger number of flaws exists, the linkage between flaws will be quicker, and the ductility lower (as observed in the highest gage length of 40 mm).

A typical pull-out force-slip curve is shown in Figure 2. Four distinct regions are indentified by roman numerals. Region I corresponds to the elastic-linear range with a rapid rate of ascent of the load. As the load increases beyond the linear region, a degree of nonlinearity is observed and this range is designated as Region II which defines the initial point of fiber debonding. The peak response is reached at region III under partial debonding conditions, where the pull-out force reaches a maximum value (P_{au}). The slip of the fiber at this point is defined as the slip at the peak and can be considered as the critical debonded length. The peak pull-out force depends on the embedded length, diameter of the fiber and the curing period, the mix design being constant. The nominal shear strength computed at P_{au} is defined as the adhesional strength (τ_{au}). In region IV the load drops to a fixed value and remains constant thereafter. The pullout behavior in the post-peak region is governed by the

frictional shear strength of the interface and continues till the fiber is completely debonded from the interface. The shear strength at this region is defined as frictional resistant strength (τ_{fu}).
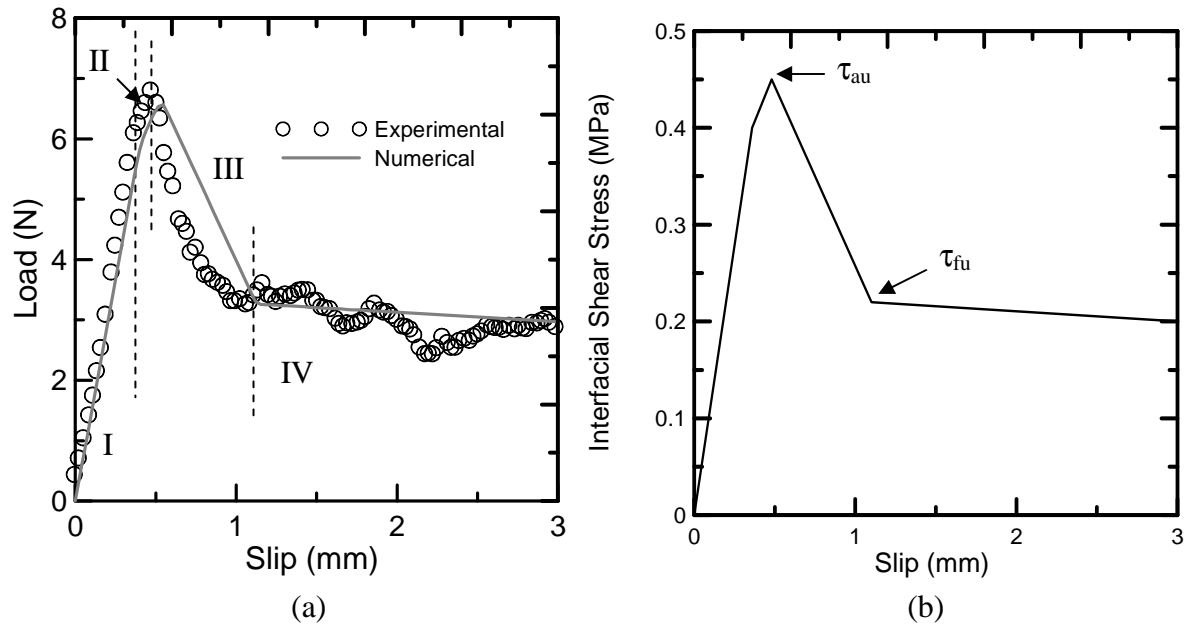

Figure 2. Fiber pull out test results of a sample tested a 3 days of curing with a embedded length of 20 mm: (a) Comparison of experimental and numerical results and (b) Interfacial constitutive relation.

Pull-out tests were carried out on embedded lengths of 10, 20, 30, and 40 mm after 3 days of curing. The results are shown in Figure 3 (a). It was found that increasing the embedded length resulted in an increase in the pull-out force from 2 to 8 N. At an embedded length of 40 mm no significant increase was observed in the pull-out force related to adhesional and frictional bond. Note that the standard deviation of the fibers tested at 30 mm was in the range as of those tested with 40 mm. As the embedded lengths were increased, a slight decrease was observed in the measurement of frictional bond strengths.

The effect of curing time from 3 to 28 days was investigated with results presented in Figure 3 (b). The bond strength reaches its maximum capacity at 14 days and the further curing of the matrix shows no effect on ages of 21 and 28 days. The average adhesional bond strength after 15 days ranged from 0.59 to 0.67 MPa. Individual values of adhesional bond strength at 14 days ranged from 0.35 to 1.29 MPa. Frictional bond strength results had less scatter with values ranging from 0.37 to 0.44 MPa after 14 days. The fiber-matrix bond strength results are in the range of some synthetic fibers. The pull out behavior of carbon fibers embedded in different cement matrices were investigated and their mean adhesional bond strength for diameters of 10 and 46 μm ranged from 0.52 to 1.29 MPa and 0.39 to 3.02 MPa, respectively [17]. Polypropylene fibers presented an adhesional bond strength of 0.5 MPa [18].
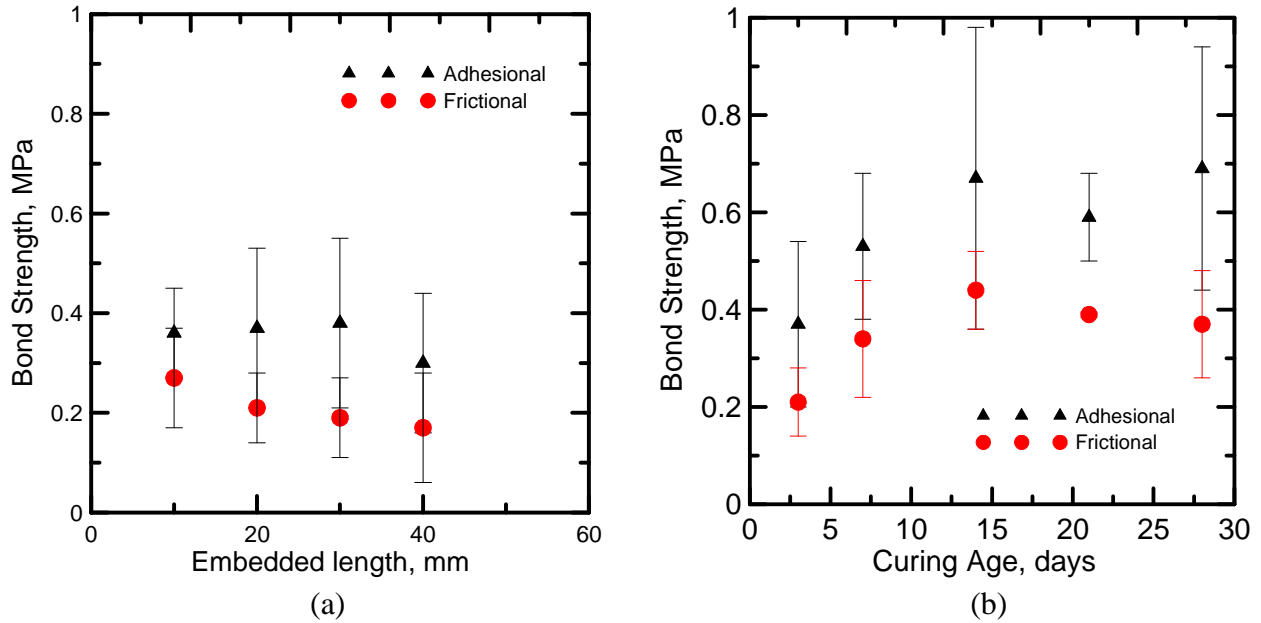
Figure 3. Influence of (a) embedded length and (b) curing age on the fiber-matrix interfacial bond strength.

Figure 4 (a) shows a typical tensile stress strain response of the sisal fiber reinforced composite system. Five distinct zones are identified using roman numerals with two zones prior to and three zones after the bend over point (BOP). Zone I corresponds to the elastic linear range where both matrix and the fiber behave linearly. Due to low volume fraction of fibers (≤ 10%) the stiffness of the composite is dominated by matrix properties and this zone is limited to strain measures of up to 150 - 175 μstr. The initial stress vs. strain response is marked by a limited range of linear elastic portion as the two strain measures are almost the same, and the specimen exhibits the highest stiffness. The linear zone is terminated by initial crack formation in the matrix phase (re-ported as of σ_{BOP}^{-} from experiments) as shown in Figure 4 (a). After the initiation of cracks in the matrix, its load carrying capacity does not vanish as the cracks are bridged by the longitudinal fibers (see Figure 4 (b)).

Immediately after the initiation of first matrix crack, other matrix cracks also initiate throughout the specimen at approximately regular intervals and begin to propagate across the width. The strain range within Zone II is associated with formation of matrix cracks, however, no single crack has traversed the entire width. The term defined as BOP^{+} corresponds to the stress level at which the first matrix crack completely propagates across the width. As indicated in the experimental results shown in Figure 4 (a) the linear behavior terminates at the σ_{BOP}^{-} = 3.63 - 4.86 MPa. The bend over point ranges from the beginning of non-linearity at 4.80 MPa to a point where the slope drastically decreases (σ_{BOP}^{+} = 4.80 - 5.59 MPa). Zone II is therefore defined as the stable cracking range between the two stress levels of σ_{BOP}^{-} and σ_{BOP}^{+}.

The post BOP stage is characterized by formation of distributed cracking in Zone III. In this homogenization phase, as the applied strain increases, more cracks form and the spacing de-creases in an exponential manner.
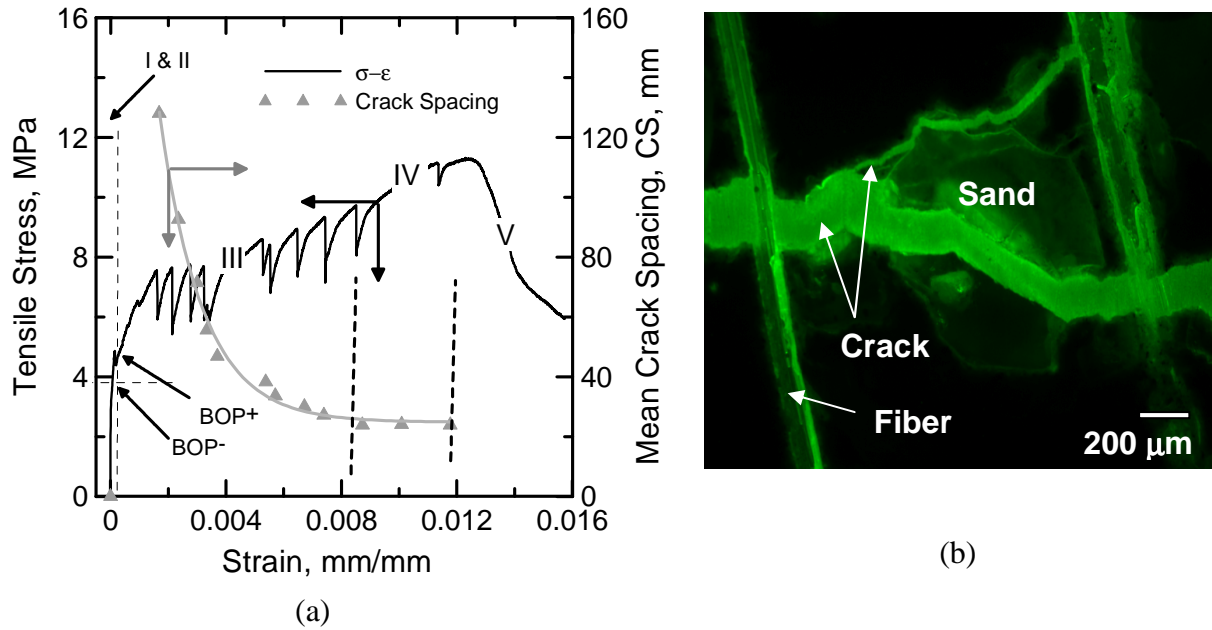
Figure 4. Tensile response of sisal fiber reinforced composite: (a) stress vs. strain curve and crack spacing analysis and (b) fluorescent micrograph showing the sisal fiber bridging matrix cracks.

The crack spacing measurements as shown in Figure 4 (a) show a general reduction in spacing during loading until a steady state condition is reached. This zone covers a range at the end of Zone II and remain constant throughout Zone IV. This constant level of crack spacing is defined as saturation crack spacing. Beyond this point, reduction in crack spacing is not observed since no new cracks are forming, and additional imposed strain results in widening of the existing cracks.

It can be seen from Figure 4 (a) that at a strain of 0.0016 mm/mm (Zone III) the cracking spacing drastically decreases from an initial value of 130 mm to 45 mm. During the multiple crack formation the crack spacing decreases until a point (beginning of Zone IV) where it becomes constant at 23 mm.

Zone IV corresponds to the completion of cracking phase and initiation of debonding. As the cracking saturates in the specimen, Zone IV is dominated by progressive damage and characterized by a crack widening stage ultimately leading to failure by fiber pullout. The average ultimate strain of the composite is 1.53 % (measured from cross-head displacement) which shows the capacity of the sisal fibers to cause crack distribution. The average ultimate strength of 12 MPa and an initial modulus of 34.17 GPa is indicative that sisal fiber reinforced cement composite presents a mechanical performance high enough for structural level applications.

Conclusions

In the present work sisal fiber reinforced cement composites were experimentally characterized in three different levels: reinforcement, interface and bulk composite. The sisal fiber presented average elastic modulus of 19 GPa and ultimate tensile strength of 400 MPa. The Weibull modulus decreased from 4.6 to 3.0 when the gage length was increased from 10 mm to 40 mm, respectively. This can be explained by the fact that the average flaw size is independent of gage length, but that the number of flaws increases with increasing volume. Thus, while average flaw size controls

strength, the number of flaws may play a more important role in controlling the strain-to-failure, since the linking of cracks at flaws determines the strain-to-failure. It follows that at larger gage lengths, the linking of flaws is easier, because of the larger number of flaws.

Pull-out test results showed that the bond strength reaches its maximum capacity at 14 days and the further curing of the matrix shows no effect on ages of 21 and 28 days. The average adhesional bond strength after 15 days ranged from 0.59 to 0.67 MPa. It was found that increasing the embedded length the pull-out force increased from approximately 2 to 8 N. At an embedded length of 40 mm no significant increase was observed in the pull-out force related to adhesional and frictional bond. No improvement in the bond strength was observed by increasing the embedded length.

The use of sisal fiber as continuous reinforcement in multi layered cementitious composites resulted in a material with multiple cracking behavior under tensile loading. The high tensile strength of the sisal fiber together with it's adequate bond strength resulted in a material with high ductility and ultimate tensile strength in the order of 12 MPa.

References

[1] Swift D.F., Smith R.B.L. The Flexural Strength of Cement-Based Composites using Low Modulus (sisal) Fibers. Composites 1979;6(3):145-148.

[2] Coutts R.S.P., Warden P.G. Sisal Pulp Reinforced Cement Mortar. Cement & Concrete Composites 1992;14(1):17-21.

[3] Toledo Filho R.D., Ghavami K., England G.L., Scrivener K. Development of Vegetable Fiber-Mortar Composites of Improved Durability. Cement & Concrete Composites 2003:25(2):185-196.

[4] Toledo Filho R.D., Scrivener K., England G.L., Ghavami K. Durability of Alkali-Sensitive Sisal and Coconut Fibers in Cement Mortar Composites. Cement & Concrete Composites 2000;22(2):127-143.

[5] Toledo Filho R. D., Joseph K., Ghavami K., England G.L. The use of Sisal Fiber as Reinforcement in Cement Based Composites. Brazilian Journal of Agricultural and Environmental Engineering 1999;3(2):245-256.

[6] Silva F.A., Ghavami K., d'Almeida J.R.M. Toughness of Cementitious Composites Reinforced by Randomly Sisal Pulps. In: Eleventh International Conference on Composites Engineering. Hilton Head Island, 2004.

[7] Silva F.A., Ghavami K., d'Almeida J.R.M. Bamboo-Wollastonite Hybrid Cementitious Composites: Toughness Evaluation. In: Joint ASME/ASCE/SES Conference on Mechanics and Materials, Baton Rouge, 2005.

[8] Silva F.A., Ghavami K., d'Almeida J.R.M. Behavior of CRBP-AL Composites Subjected to Impact Load. In 17th ASCE Engineering Mechanics Conference, Delaware, 2004.

[9] Mobasher B., Pivacek A., and Haupt G. J. Cement Based Cross-Ply Laminates. Journal of Advanced Cement Based Materials 1997;6:144-152.

[10] Silva F.A., Melo Filho J.A., Toledo Filho R.D., Fairbairn E.M.R. Effect of Reinforcement Ratio on the mechanical response of compression molded sisal fiber textile reinforced concrete. In: High Performance Fiber Reinforced Cement Composites (HPFRCC5), Mainz, p. 175-182, 2007.

[11] Hagger J., Will N., Aldea C., Brameshuber W., Brockmann T., Curbach M., Jesse J. Applications of Textile Reinforced Concrete. In: Brameshuber, W. (edited) State-of-the-Art Report of Rilem Technical Committee 201-TRC: Textile Reinforced Concrete. 2006, p.237-266.

[12] Toledo Filho R.D., Silva F.A., Fairbairn E.M.R., Melo Filho J.A. Durability of compression molded sisal fiber reinforced mortar laminates. Construction and Building Materials 2009;23:2409-2420.

[13] Brazilian Standard NBR 11578, Cimento Portland Composto. Associação Brasileira de Normas Técnicas (ABNT), 1991 (In Portuguese).

[14] Silva F.A., Chawla N., and Toledo Filho R.D. Tensile behavior of high performance natural (sisal) fibers. Composites Science and Technology 2008;68:3438-3443.

[15] Silva F.A., Mobasher B., Toledo Filho R.D. Cracking mechanisms in durable sisal reinforced cement composites. Cement and Concrete Composites 2009;31: 721-730.

[16] Chawla K.K.. Ceramic Matrix Composites. Chapman & Hall, London, 1993.

[17] Katz A., Li V.C., Kazmer A. Bond Properties of Carbon Fibers in Cementitious Matrix. Journal of Materials in Civil Engineering 1995;7:125-128.

[18] Singh S., Shukla A., Brown R. Pullout behavior of polypropylene fibers from cementitious matrix. Cement and Concrete Research 2004;34:1919-1925.